Extension of an immersed boundary method for large eddy simulation of turbulent flows

Tianmei Pu and Chunhua Zhou*

Department of Aerodynamics,
Nanjing University of Aeronautics and Astronautics,
Nanjing 210016, China
Email: 1005102227@qq.com
Email: chzhou@nuaa.edu.cn
*Corresponding author

Abstract: In this paper, an immersed boundary method is extended to large eddy simulation of turbulent flows. For the interior nodes in the immediate vicinity of the immersed wall, some of their neighbouring nodes are in the solid phase, and the flow variables at these interior nodes cannot be calculated by solving the governing equations. In the present immersed boundary method, the flow variables at these nodes are determined via an approximate form of solution involving the boundary condition. A wall model based on the simplified turbulent boundary layer equations is introduced to alleviate the requirement of mesh resolution in the near-wall region. The wall shear stress prescribed by the wall modelling technique and the no-penetration condition are enforced at the immersed boundary to evaluate the velocity at an interior node in the immediate vicinity of the wall. A dynamic subgrid-scale model is adopted in the framework of the immersed boundary approach. Several numerical experiments have been conducted to verify the ability of the present method. The predicted results agree well with the published experimental or numerical data.

Keywords: immersed boundary method; turbulent flows; wall modelling; large eddy simulation; LES; dynamic subgrid-scale model.

Reference to this paper should be made as follows: Pu, T. and Zhou, C. (2021) 'Extension of an immersed boundary method for large eddy simulation of turbulent flows', *Progress in Computational Fluid Dynamics*, Vol. 21, No. 3, pp.129–140.

Biographical notes: Tianmei Pu is currently a PhD student in the Department of Aerodynamics, NUAA. Her research area is CFD.

Chunhua Zhou received his PhD from NUAA in 1993 and PhD from Université Paris VI. Currently, he serves NUAA and he is a Professor in the Department of Aerodynamics, NUAA. His research area is CFD and numerical analysis.

1 Introduction

For practical applications, generation of high quality body-fitted meshes may be time-consuming and need a high level of expertise. Furthermore, transient re-meshing strategies required in the simulation of moving-boundary flows increase the difficulty of mesh generation. The immersed boundary (IB) method has provoked enormous interest due to its easy mesh generation both for complex configurations and for moving boundary problems.

The IB method was first introduced in the early '70s by Peskin (1972) and has been applied in a variety of problems. Detailed discussions of different techniques can be found in Iaccarino and Verzicco (2003) and Mittal and Iaccarino (2005). Most of the published applications of IB methods are for Euler and laminar flows (Zhou and Shu, 2011; Zhang and Zhou, 2014; Senturk et al., 2019), and only a few focus on simulations of turbulent flows (Tessicini et al., 2002; Sarkar and Sarkar, 2010; Capizzano, 2011). Large eddy simulation (LES) is a cost-effective approach for simulation of turbulent flows, in which the governing equations are spatially filtered to resolve the dynamics of the large scales and modelling is done only for the 'universal' small scales. A wall-resolved LES needs to represent the near-wall anisotropy of turbulence which requires a high mesh resolution, scaling with the squared friction Reynolds number Re_τ^2 (Baggett et al., 1997). Due to its isotropic property, the node number of the Cartesian mesh used by an IB method for wall-resolved LES will be extremely large. Even if a local refinement strategy is adopted, the total number of the mesh nodes is still very large. Wall modelling technique is one way to overcome this difficulty. Conventional approaches in wall modelling focus on imposing synthetic boundary conditions by prescribing wall shear stress instead of no-slip velocity (Cabot and Moin, 2000).

Earlier wall models are based on the existence of a logarithmic law of the wall. This method was first applied in simulating a channel flow by Schumann (1975). A number of modifications to Schumann's model have been made by Werner and Wengle (1991) to eliminate the need for a *priori* prescription of the mean wall shear stress and to simplify its implementation. Recently, more accurate wall models have been developed. Balaras et al. (1996) proposed a wall model based on simplified turbulent boundary layer equations (TBLEs). In this approach, the simplified TBLEs are solved on a fine one-dimensional grid embedded between the wall and the first grid point. Following the work of Balaras et al. (1996), Ng et al. (2004) incorporated the TBLEs-based wall model in the RANS simulation of flows in turbomachinery. The yielded wall shear stress is provided as the boundary condition of the outer layer. Most of the reported LES with a wall model are for body-fitted-mesh methods, while its application to an IB method has not been thoroughly explored. In the work of Tessicini et al. (2002), an equilibrium wall model based on the simplified TBLEs was proposed for the LES-IB application, along with an operative procedure for the reconstruction of the wall shear stress in the IB framework. The performance of a TBLEs-based wall model was analysed by Chen et al. (2014) in LES with a cut-cell method. More recently, in the work of Shi et al. (2019), TBLEs-based wall model and Werner-Wengle wall model (Werner and Wengle, 1991) was implemented in the diffuse-interface direct-forcing IB method and the proposed method was validated by the benchmark simulation of flows around DARPA SUBOFF.

The hybrid Cartesian/immersed boundary (HCIB) method was suggested by Gilmanov et al. (2003). In this method, the IB is treated as a sharp interface and the velocity is reconstructed at the interior grid nodes closest to the IB to provide boundary conditions for the discrete governing equations. Borazjani and Sotiropoulos (2008) applied it to investigate the hydrodynamics of fish swimming. It was then extended by Borazjani (2013) to the simulation of fluid-structure interaction of heart valve tissue. Deleon et al. (2018) proposed a HCIB-like method, and applied it to wall-modelled LES simulations of flow over the complex terrain of Askervein and Bolund Hills under neutrally-stratified conditions. All the IB methods in Borazjani and Sotiropoulos (2008), Borazjani (2013) and Deleon et al. (2018) were implemented in the frame of finite difference. Zhang and Zhou (2014) proposed an HCIB-like method for inviscid compressible flows, in which a finite volume approach was employed for spatial approximation. This HCIB-like method was then extended to RANS simulation of turbulent flows by Pu and Zhou (2018). Compared to the ghost-cell method (Dadone and Grossman, 2007) or the local domain-free discretisation method (Zhou and Shu, 2011), where the forcing nodes are located inside the solid phase, one obvious advantage of the HCIB method (Borazjani and Sotiropoulos, 2008; Borazjani, 2013) and the HCIB-like method (Zhang and Zhou, 2014; Deleon et al., 2018; Pu and Zhou, 2018) is that the tedious task of handling the multi-valued points (usually located in the vicinity of thin surface or sharp corners) can be avoided.

In this work, the HCIB-like approach proposed in Zhang and Zhou (2014) and Pu and Zhou (2018) is extended to LES. A TBLEs-based wall model is employed to lessen the requirement of the near-wall mesh resolution. In the finite-difference IB method of Deleon et al. (2018), a log-law-based wall model is employed to alleviate the near-wall mesh resolution and this kind of wall model indicates that the first off-wall nodes should be located in the logarithmic layer. The TBLEs-based wall model can remove this constraint. Compared to the finite-difference approximation, the finite-volume approximation employed in the present method, which is widely used in engineering, allows the use of unstructured meshes and makes mesh adaptation become easy. So, the proposed IB/wall modelling approach can be readily implemented in a code for engineering application.

The remainder of this paper is arranged as follows. In Section 2, the governing equations and the basic numerical schemes are described. Section 3 discusses in detail the evaluation of flow variables at the near-wall interior nodes. In Section 4, numerical experiments are performed to scrutinise the capability of the present LES-IB method by comparing the predicted results with the published experimental data or numerical results. Finally, the summary and conclusions of this paper are given in Section 5.

2 Governing equations and basic schemes of numerical approximation

In this work, an incompressible fluid with constant density and viscosity is considered. Employing a subgrid-scale model (Germano et al., 1991), the filtered N-S equations can be written in the following non-dimensional form,

$$\mathbf{I}^m \cdot \frac{\partial \mathbf{w}}{\partial t} + \frac{\partial \mathbf{f}_i}{\partial x_i} = \frac{\partial \mathbf{g}_i}{\partial x_i} \tag{1}$$

where $\mathbf{w}$, $\mathbf{f}_i$ and $\mathbf{g}_i$ are the vectors of flow variables, convective fluxes and viscous fluxes, respectively,

$$\begin{aligned} \mathbf{w} &= \begin{bmatrix} \overline{p} \\ \overline{u}_1 \\ \overline{u}_2 \\ \overline{u}_3 \end{bmatrix}, \mathbf{f}_i = \begin{bmatrix} \overline{u}_i \\ \overline{u}_1\overline{u}_i + \overline{p}\delta_{1i} \\ \overline{u}_2\overline{u}_i + \overline{p}\delta_{2i} \\ \overline{u}_3\overline{u}_i + \overline{p}\delta_{3i} \end{bmatrix}, \\ \mathbf{g}_i &= \frac{1}{\mathrm{Re}}\left(1+\nu_t/\nu\right)\cdot \begin{bmatrix} 0 \\ 2\overline{S}_{i1} \\ 2\overline{S}_{i2} \\ 2\overline{S}_{i3} \end{bmatrix}, \end{aligned} \tag{2}$$

and $\mathbf{I}^m$ is the modified identity matrix annihilating the temporal derivative of pressure from the continuity equation,

$$\mathbf{I}^m = \begin{bmatrix} 0 & 0 & 0 & 0 \\ 0 & 1 & 0 & 0 \\ 0 & 0 & 1 & 0 \\ 0 & 0 & 0 & 1 \end{bmatrix}. \tag{3}$$

In equation (2), $\overline{u}_i$ denotes the filtered Cartesian velocity component, $\overline{p}$ the filtered pressure (divided by the constant density), ν the molecular viscosity which is unit, ν_t the eddy viscosity, δ_{ij} the Kronecker's delta, Re and $\overline{S}_{ij}$ the Reynolds number and the strain-rate tensor, respectively

$$\mathrm{Re} = \frac{UL}{\nu}, \overline{S}_{ij} = \frac{1}{2}\left(\frac{\partial \overline{u}}{\partial x_j} + \frac{\partial \overline{u}_j}{\partial x_i}\right), \tag{4}$$

where U is the reference velocity and L the reference length of the considered problem.

The subgrid-scale viscosity ν_t is modelled to be $\nu_t = C_s \overline{\Delta}^2 |\overline{S}|$, where $|S| = \sqrt{2\overline{S}_{ij}\overline{S}_{ij}}$ is the magnitude of the strain-rate tensor, $\overline{\Delta}$ the filter width and C_s the model coefficient. In this wok, C_s is determined dynamically by the Lagrangian averaging procedure proposed by Meneveau et al. (1996). This averaging procedure allows the application of the subgrid-scale model to complex flows that do not possess homogeneous directions.

$\Omega \subset R^3$ is a connected open set containing a solid object, which is discretised by a tetrahedral mesh. The governing equations are discretised with the Galerkin finite element approach (Mavriplis and Jameson, 1990) on the unstructured colocated mesh. Employing the concept of a lumped mass matrix, the finite-element approximation in Mavriplis and Jameson (1990) is equivalent to a finite volume approximation. The semi-discrete form of the governing equation (1) at K can be obtained,

$$\begin{aligned} \mathbf{I}^m \cdot \Omega_K \left(\frac{\partial \mathbf{w}}{\partial t}\right)_K &= -\sum_{e=}^{n_e} \frac{\mathbf{F}^A + \mathbf{F}^B + \mathbf{F}^C}{3} \cdot \Delta \mathbf{S}_{ABC} \\ &+ \sum_{e=1}^{n_e} \frac{4}{3} \mathbf{G}^e \cdot \Delta \mathbf{S}_{ABC}, \end{aligned} \tag{5}$$

where $\mathbf{F}$ and $\mathbf{G}$ denote the inviscid and viscous flux tensor, respectively, n_e the number of all the tetrahedrons around K (the control volume of node K) and Ω_K the volume sum of these tetrahedrons. As pictured in Figure 1, $\Delta \mathbf{S}_{ABC}$ represents the directed (outward normal) area of the triangular face opposite to the vertex K, $\mathbf{F}^A$, $\mathbf{F}^B$, and $\mathbf{F}^C$ are the inviscid flux tensors at the three vertices, and $\mathbf{G}^e$ is the viscous flux that is constant over each tetrahedron.

Equation (5) can be rewritten in the following ordinary differential equation

$$\mathbf{I}^m \cdot \Omega_K \left(\frac{d\mathbf{w}_K}{dt}\right)^{n+1} + R_K\left(\mathbf{w}^{n+1}\right) = 0. \tag{6}$$

Employing a third-order temporal discretisation, equation (6) becomes (Zhou and Shu, 2011)

$$\begin{aligned} &\mathbf{I}^m \left[\Omega_K \frac{\beta_1 \mathbf{w}_K^{n+1} + \beta_2 \mathbf{w}_K^n + \beta_3 \mathbf{w}_K^{n-1} + \beta_4 \mathbf{w}_K^{n-2}}{\Delta t}\right] \\ &+ R_K\left(\mathbf{w}^{n+1}\right) = \overline{R}_K\left(\mathbf{w}^{n+1}\right) = 0, \end{aligned} \tag{7}$$

where $\beta_1 = \frac{11}{6}, \beta_2 = -3, \beta_3 = \frac{3}{2}, \beta_4 = -\frac{1}{3}$. A derivative with respect to a pseudo time τ is added to equation (7) to give

$$\Omega_K \frac{d\mathbf{w}_K^{n+1}}{d\tau} + \overline{R}_K\left(\mathbf{w}^{n+1}\right) = 0. \tag{8}$$

At each physical time step, the solution of equation (8) is found by marching to a steady state in pseudo time, and then the solution of equation (6) is obtained. A five-stage, point-implicit scheme is used for pseudo-time marching. More details can be found in reference (Zhou and Shu, 2011; Pu et al., 2019).

Figure 1 Directed area of influence-domain-boundary face of a tetrahedron

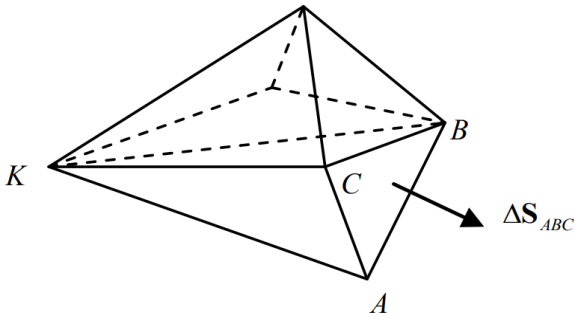

The method of artificial compressibility is employed to convert the hyperbolic-elliptic unsteady incompressible Navier-Stokes equations into a hyperbolic-parabolic system and to reduce the disparity in sound and convective waves. Following the work of Belov et al. (1997), a local precondition matrix is introduced to yield

$$\Omega_K \frac{d\mathbf{w}_K^{n+1}}{d\tau} + \mathbf{Pr} \cdot \overline{R}_K\left(\mathbf{w}^{n+1}\right) = 0, \tag{9}$$

where

$$\mathbf{Pr} = diag\left(\beta^2, 1, 1, 1\right). \tag{10}$$

The local artificial compressibility parameter β is taken as (Nithiarasu, 2003):

$$\beta^1 = \max\left(0.25, v_{conv}^2, v_{diff}^2\right), \tag{11}$$

where $v_{conv} = \sqrt{u_i u_i}$ is the convective velocity and $v_{diff} = 2 / (hRe)$ the diffusion velocity.

The Galerkin finite-element approximation is equivalent to the central difference. To prevent odd-even decoupling, stemming from the central differencing of convective term, the following artificial dissipation operator (Belov et al., 1997) is adopted

$$D_K(\mathbf{w}) = -\mathbf{Pr}^{-1} \cdot \sum_{i=1}^{n_i} \varepsilon \frac{\alpha_K + \alpha_i}{2} \left(\nabla^2 \mathbf{w}_K - \nabla^2 \mathbf{w}_i \right), \tag{12}$$

where ε is an empirical coefficient, taken to be 1/128, α is a factor proportional to an isotropic value of the maximum eigenvalue at each node (Mavriplis and Jameson, 1990), and n_i represents the number of edges meeting at node K. The undivided Laplacian of $\mathbf{w}$ at K can be approximated as

$$\nabla^2 \mathbf{w}_K = \sum_{i=1}^{n_i} \left(\mathbf{w}_i - \mathbf{w}_K \right). \tag{13}$$

3 Treatment of the IB

According to the spatial discretisation described in Section 2, the flow variables at any mesh node depend on those at the neighbouring nodes connected to this node by a cell edge. Therefore, for the points that have at least one neighbouring point outside the solution domain, the flow variables cannot be evaluated by solving the discretised governing equations. These nodes are called IB nodes in this work. All the mesh nodes are categorised into IB nodes, interior computed nodes at which the flow variables are calculated by solving the governing equations, and exterior nodes that locate in the solid phase and are blanked out of computation. As shown in Figure 2, B is an IB node and the flow variables at B will be determined via the approximate form of solution, which involves the boundary condition.

Figure 2 IB model

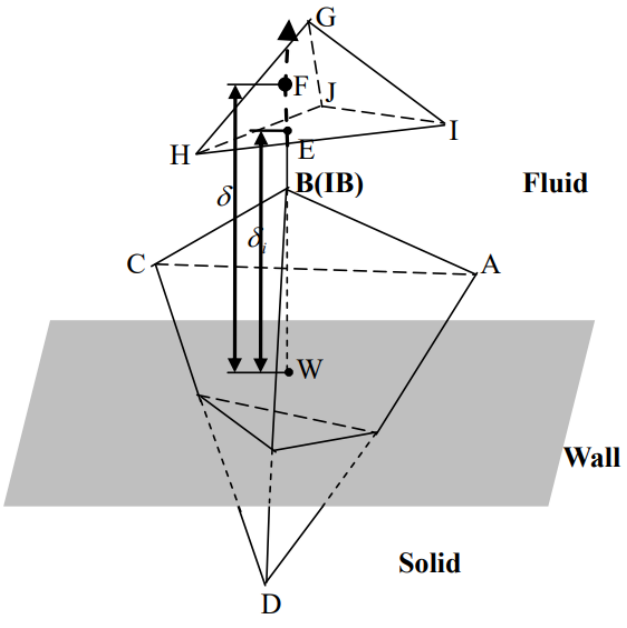

Notes: B: immersed boundary node; W: wall-normal intersection; E: face-normal intersection; F: reference point for B.

In order for LES to be accurate for wall-bounded turbulent flows, the mesh in the near-wall region must be fine enough since the length scale of the energy-containing eddies gets progressively smaller toward the wall. Due to its isotropic property, the node number of Cartesian mesh used in an IB method that meets this requirement will be extremely large. The wall modelling technique alleviates the requirement of mesh resolution near the wall by skipping the inner layer of the turbulent flow. In the present work, the wall model based on the simplified TBLEs (Balaras et al., 1996) is introduced to feed LES with approximate wall boundary conditions. Instead of the no-slip condition used in the wall-resolved LES, the velocity components at the IB nodes are evaluated by using the no-penetration condition and the wall shear stress yielded by the wall model.

To calculate the flow variables at a given IB node via the approximate form of solution, a reference point inside the solution domain is needed. With reference to Figure 2, the determination of the reference point is described as follows. First, the intersection W between the normal line and the wall and the intersection E between the normal line and the nearest-to-wall triangular face are calculated. Three vertices of the nearest-to-wall face are all interior computed nodes. The distance between the intersections W and E is denoted by δ_i and then a constant $\delta = \max_{i=1,N_B} \delta_i$ can be obtained, where NB is the total number of the IB nodes. As shown in Figure 2, the point F on the normal line with a distance δ from the solid wall is defined as the reference point for the IB node B. In this definition, the distance of all the reference points to the wall is constant, which is favourable to produce a smoother result in the vicinity of the IB. The flow variables at a reference point can be obtained via a linear interpolation over its host tetrahedron (*HIJG* in Figure 2).

According to the no-penetration condition, the linear interpolation gives the normal velocity at the IB node B

$$\tilde{v}_B = \frac{\tilde{v}_F \, |WB| + \tilde{V}_W \, |BF|}{|WF|}, \tag{14}$$

where $\tilde{V}_W$ is the normal velocity of the body at W, and $\tilde{v}_F$ and $\tilde{v}_B$ are normal velocities at the reference point F and the IB node B, respectively. For a stationary body, $\tilde{V}_W = 0$.

The following simplified inviscid momentum equation in the normal-to-wall direction is considered in the evaluation of pressure at the IB node B,

$$\frac{\partial p}{\partial n} = -\left(\frac{d\mathbf{u}}{dt} \right)_\gamma \cdot \mathbf{n} \tag{15}$$

where $\mathbf{u}$ is the velocity vector of fluid, γ the wall, $\mathbf{n}$ the unit outward vector normal to the wall. Using the no-penetration condition, the pressure at B is

$$p_B = p_F + |BF| \left(\frac{d\tilde{V}}{dt} \right)_W \tag{16}$$

where $\tilde{V}$ denotes the normal velocity of body motion, and p_F the pressure at F. For stationary body, $\tilde{V} = 0$, and then

$$p_B = p_F \tag{17}$$

The tangential velocities at the IB node B is evaluated via the wall shear stress which is yielded by the wall modelling technique. The wall model adopted in this work is based on the TBLEs,

$$\frac{\partial}{\partial n}\left[(\nu+\nu_t)\frac{\partial \tilde{u}_i}{\partial n}\right]=S_i,\quad i=1,2 \tag{18}$$

with n the direction normal to the wall, $\tilde{u}_i$ the tangential velocity, and S_i the sum of the unsteady, convective, and pressure gradient terms. In Capizzano (2011), the wall model needs to be solved in two tangential directions. Here, a modified local coordinate system (Zhou and Shu, 2009) is employed to transform the three-dimensional problem into a local 'two-dimensional' one. As illustrated in Figure 3, the local system is composed of the streamwise direction η, the wall-normal direction n, and the binormal direction ζ, which is perpendicular to the $\eta - n$ plane. The streamwise direction η is approximated to be the projection of the velocity direction at the reference point onto the body surface, which means that the velocity component at the reference point in ζ-direction is equal to zero. In such local coordinate system, the TBLEs [equation (18)] are solved only in η-direction and the computational cost can be reduced, compared to the treatment of Capizzano (2011). The tangential direction mentioned below is referred to the η-direction

Figure 3 Local coordinate system

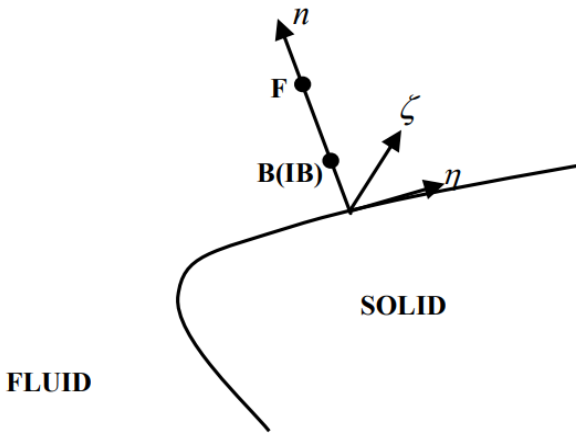

For simplicity, the equilibrium stress model is adopted in this work, i.e., S_i = 0 in equation (18). In the local coordinate system, integrating equation (18) from the reference point to the wall with no-slip boundary condition imposed, one can obtain the wall shear stress,

$$\tau_w=\mu\left.\frac{\partial \tilde{u}}{\partial n}\right|_{y=0}=\frac{u_F}{\int_0^{\delta}\frac{dy}{\nu+\nu_t}}, \tag{19}$$

where $\tilde{u}_F$ is the tangential velocity at the reference point F, and the eddy viscosity ν_t is calculated via the van Driest damping function,

$$\frac{\nu_t}{\nu}=\kappa y^+\left(1-e^{-y^+/A}\right)^2, \tag{20}$$

with κ = 0.4, A = 19 and $y^+=y\sqrt{\tau_w}/\nu_w$. The system of (19) and (20) is solved iteratively in terms of τ_w. The shear wall stress τ_w can also be approximated as

$$\tau_w\approx(\nu_F+\nu_{t,F})\frac{\tilde{u}_F-\tilde{u}_B}{|BF|}, \tag{21}$$

where ν_F and $\nu_{t,F}$ are the molecular and eddy viscosity at F, respectively. Then, $\tilde{u}_B$, the tangential velocity at the IB node B, can be obtained

$$\tilde{u}_B=\tilde{u}_F-\frac{|BF|}{\nu_F+\nu_{t,F}}\tau_w. \tag{22}$$

The Cartesian velocity components at an IB node can be obtained directly with the known normal and tangential components.

In LES, the eddy viscosity ν_t at an IB node is obtained by using its profile in the vicinity of the wall

$$\frac{\mu_t}{\mu_w}=\kappa e^{-\kappa B}\left[e^{\kappa u^+}-1-\kappa u^+-\frac{(\kappa u^+)^2}{2}\right]. \tag{23}$$

4 Numerical experiments

To validate the present LES-IB method, various turbulent flows are simulated. All the used tetrahedral meshes are obtained by dividing the hexahedral cells of Cartesian meshes. The results obtained by the present method are labelled as 'LES/IB_WM' in the subsequent figures. The application of wall modelling technique dictates that the near-wall mesh resolution must be smaller than the boundary thickness. Successive refinement of the three dimensional LES mesh will lead to a dramatic increase of node number, and the extremely large computational cost makes the test of grid convergence of LES very difficult. In addition, the solution of implicitly filtered LES is sensitive to the numerical grid used (Bose et al., 2010). For some LES solution, grid refinement causes the agreement with direct numerical simulation or experimental data to deteriorate (Bose et al., 2010).

4.1 Flow around a circular cylinder at Re = 3900

In this subsection, the turbulent flow over a stationary circular cylinder is simulated. The Reynolds number is based on the diameter D and the velocity of free stream U. The computational domain is 30D, 20D, πD in the streamwise (x –), crosswise (y –) and spanwise (z –) directions, respectively. The coarse mesh size in the vicinity of the cylinder is Δx = 0.015, Δy = 0.014 and Δz = 0.012. The total number of the computational nodes is 636,862 and

the non-dimensional time step size is set to be 0.01. Another mesh with higher resolution of $\Delta x = 0.008$, $\Delta y = 0.007$ and $\Delta z = 0.006$ is also adopted to investigate the effects of grid resolution. For the fine mesh, the total number of the computational nodes is 1,798,726 and the time step is set to be 0.005. On the far-field boundary, non-reflecting far-field boundary conditions are employed and periodicity is imposed in the spanwise direction. In Table 1 and figures, the results obtained on the coarse and fine meshes are labelled as 'LES/IB_WM_C' and 'LES/IB_WM_F', respectively.

Table 1 Integral results of the cylinder flow computation

	$\overline{c}_d$	$-\overline{c}_{pb}$	Lr/D	St
LES/IB_WM_C	1.06	0.87	1.31	0.217
LES/IB_WM_F	1.03	0.88	1.30	0.215
DNS (Ma et al., 2000) (case 1)	–	0.96	1.12	0.203
LES (Meyer et al., 2010)	1.07	1.05	1.18	0.22
Exp (Lourenco and Shih, 1993)	0.99 ± 0.05	0.90 ± 0.05	1.33 ± 0.05	0.215 ± 0.005
Exp (Parnaudeau et al., 2008)	–	–	1.51	0.208

Figure 4 (a) Mean streamwise velocity, (b) mean transverse velocity, (c) streamwise velocity fluctuations, and (d) transverse velocity fluctuations at different streamwise locations in the wake of the circular cylinder (see online version for colours)

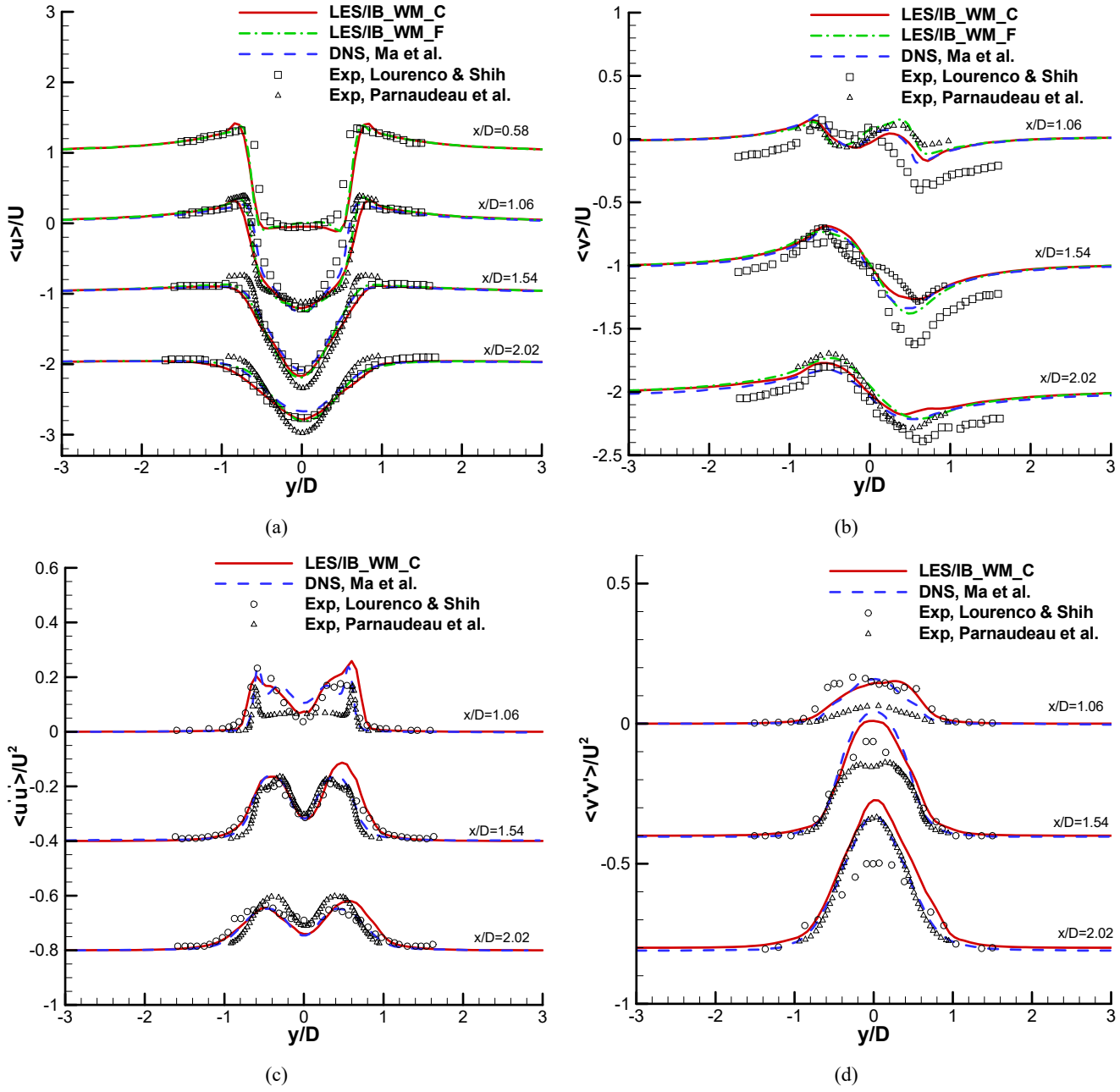

First, the integral results, such as the mean drag coefficient $\overline{c}_d$, the mean back pressure coefficient $\overline{c}_{pb}$, the mean recirculation length L_r, and the Strouhal number St are presented in Table 1, together with the referenced DNS results of Ma et al. (2000), LES results of Meyer et al. (2010), experimental data of Lourenco and Shih (1993), and experimental data of Parnaudeau et al. (2008). Overall, the present results fall in the range of the experimental data and are comparable to the referenced DNS or LES results. The mean drag coefficient obtained with the fine mesh is closer to the experimental data of Lourenco and Shih, than that obtained with the coarse one. For further quantitative validation, profiles of mean velocity components and velocity fluctuations at different streamwise locations in the wake are illustrated in Figure 4. For comparison, DNS results (case 1) (Ma et al., 2000), experimental data (Lourenco and Shih, 1993; Parnaudeau et al., 2008) are also plotted in the figures. Generally, the predicted results of the present LES/IB method with both coarse and fine meshes are close to each other and agree well with the referenced DNS results. In Figure 4(a), we can see that the V-shape velocity profile at $x / D = 1.06$ predicted by the present method is very close to the DNS result and the experimental result of Lourenco and Shih (1993), in contrast with the U-shape profile obtained by the experiment of Pamaudeau et al. (2008). The DNS simulations (Ma et al., 2000) show that with a computational domain of smaller spanwise length, the U-shape profile of stream velocity is obtained and the U-shape profile corresponds to small fluctuations in the near wake.

4.2 Turbulent flows over periodic hills

In this subsection, turbulent flows at Re = 2,800 and 10,595 in a channel with periodic hills are simulated. The definition of Reynolds number is based on the hill height H and the bulk velocity U_B at the hill crest. Figure 5 is a sketch map of the geometry of the channel with periodic hills. The computational domain is $9H \times 3.035H \times 4.5H$ in the streamwise (x), vertical (y) and spanwise (z) directions, respectively. Periodicity is imposed in the streamwise and spanwise directions. Simulation without wall modelling is also performed on the same mesh and the no-slip conditions are enforced on the IB. The results obtained without wall modelling are labelled as 'LES/IB' in the figures. For all the computations, the non-dimensional physical time-step is set to be 0.005.

Figure 5 Sketch map of the geometry of the channel with periodic hills

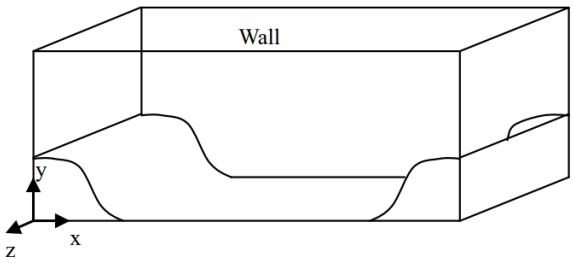

Figure 6 Instantaneous vortex structure at $t = 75$ visualised by using iso-surfaces of $Q = 1.5$, colored by the eddy viscosity (see online version for colours)

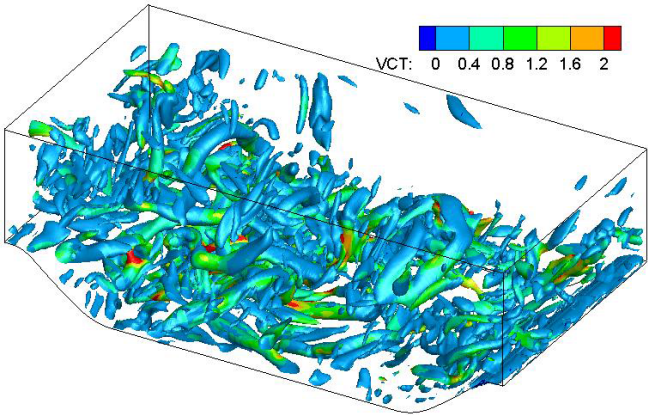

For the turbulent flow at Re = 2,800, a 305 × 96 × 64 grid with $\Delta x / H = 0.03$, $\Delta y / H = 0.032$ and $\Delta z / H = 0.071$ is used. The grid is uniform in all the directions. Figure 6 is the vortex structure at $t = 75$, visualised by using iso-surface of $Q = 1.5$. The predicted mean velocity components and shear stress at different locations are shown in Figures 7, 8 and 9 together with the DNS data of Breuer et al. (2009). Overall, the results predicted by the present LES/IB method with wall modelling are comparable to the DNS data of Breuer et al. (2009). The streamwise velocities in the wall-modelling case are closer to the referenced DNS data than those in the non-wall-modelling case, especially near the upper wall. For the vertical velocity and shear stress, the superiority of the wall modelling technique is not so obvious. This may be due to their small values which are more susceptible to the measurement uncertainties.

For the turbulent flow at Re = 10,595, a 213 × 140 × 64 grid is adopted. The grid is uniform in the spanwise direction and is stretched in the streamwise and vertical direction, with $\Delta x = 0.032$, $\Delta y = 0.016$ and $\Delta z = 0.071$ near the hills. Figures 10 and 11 show the predicted profiles of mean streamwise and vertical velocities, respectively, for which both experimental and wall-resolved LES data are available (Breuer et al., 2009). Overall, for the mean streamwise velocity, the results obtained with wall modelling are closer to the experimental data. For the profiles of the vertical velocity, better results can be obtained with the wall modelling at $x / h = 6$. However, it can be obviously seen from Figures 11(a) and 11(b) that the present LES results underestimate the mean transverse velocity at $x / h = 0.5$ and $x / h = 2$. Since these two locations are in the separation bubble, the disparity may be due to the equilibrium wall model employed in this work. It is well-known that the equilibrium assumption is no longer valid in some flow regions, such as transitional and separated flows.

Figure 7 Mean streamwise velocity <*u*> at Re = 2,800, (a) *x* / *h* = 0.5 (b) *x* / *h* = 2 (c) *x* / *h* = 4 (d) *x* / *h* = 6 (see online version for colours)

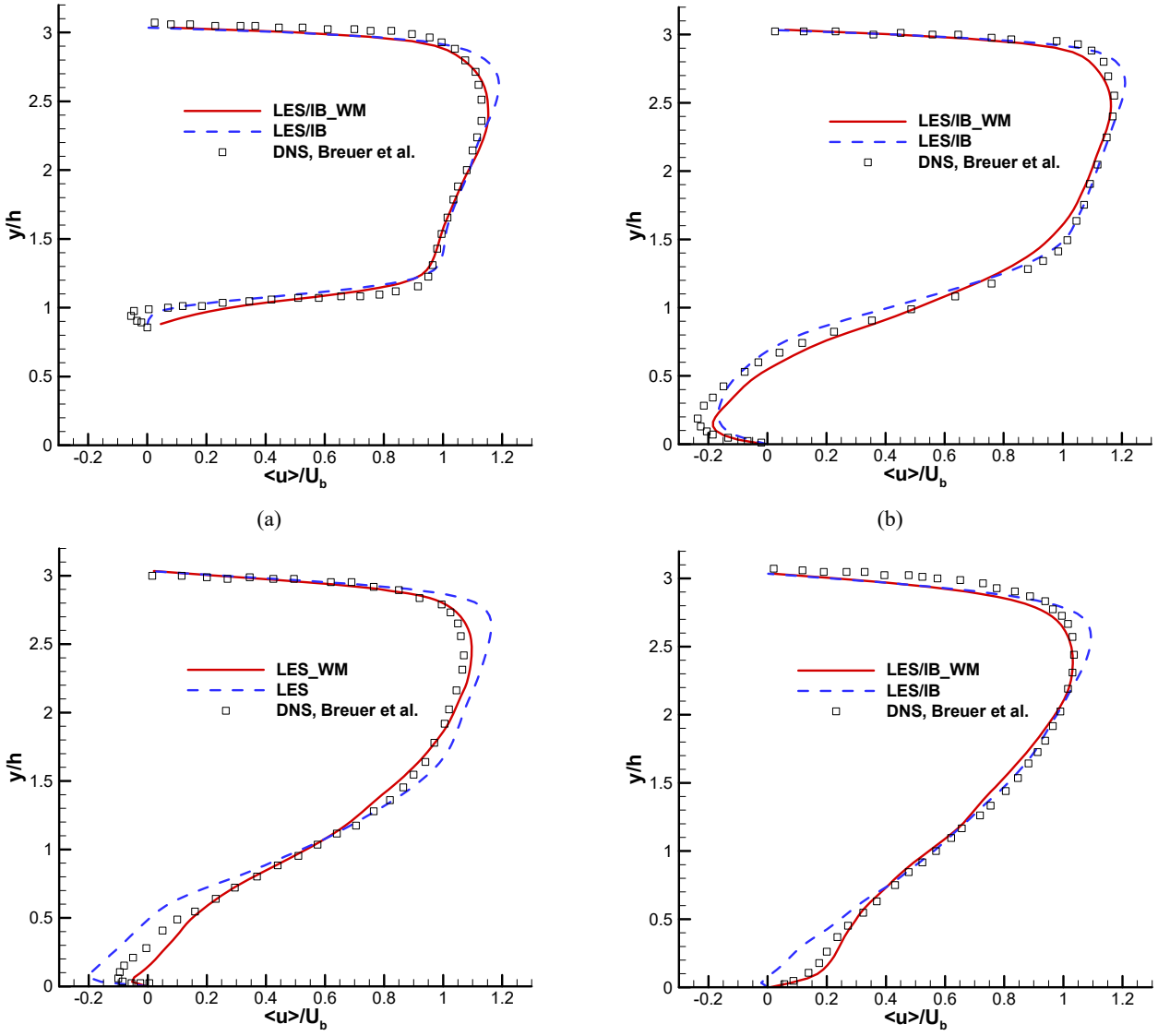

Figure 8 Mean transverse velocity <*v*> at Re = 2,800, (a) *x* / *h* = 2 (b) *x* / *h* = 4 (see online version for colours)

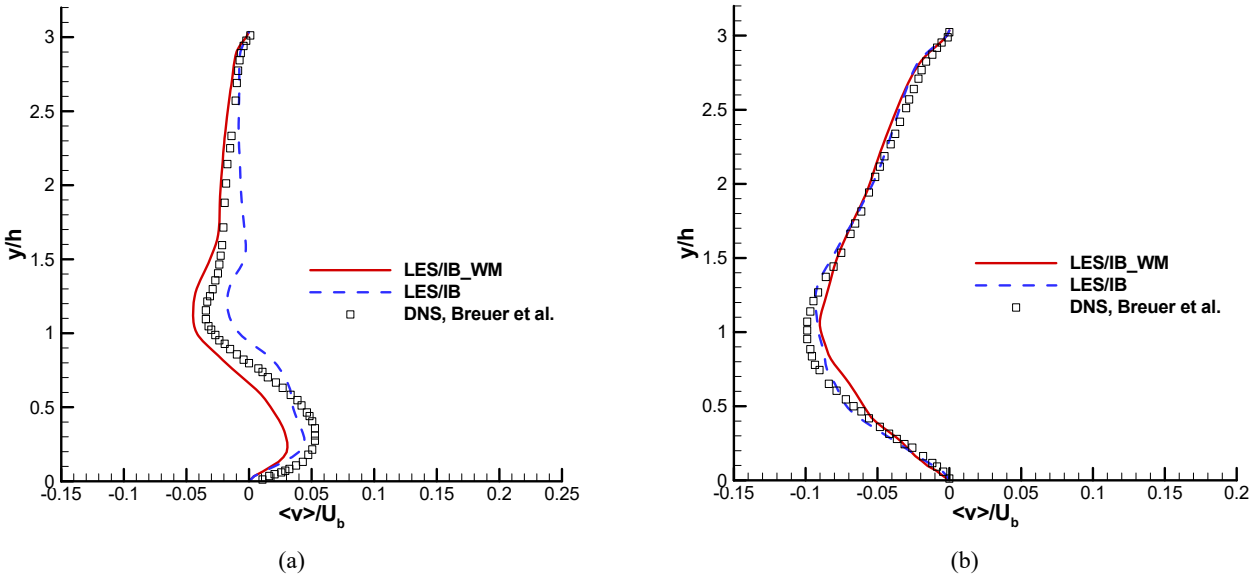

Figure 9 Shear stress $\langle u'v' \rangle$ at Re = 2,800, (a) $x / h = 2$ (b) $x / h = 4$ (see online version for colours)

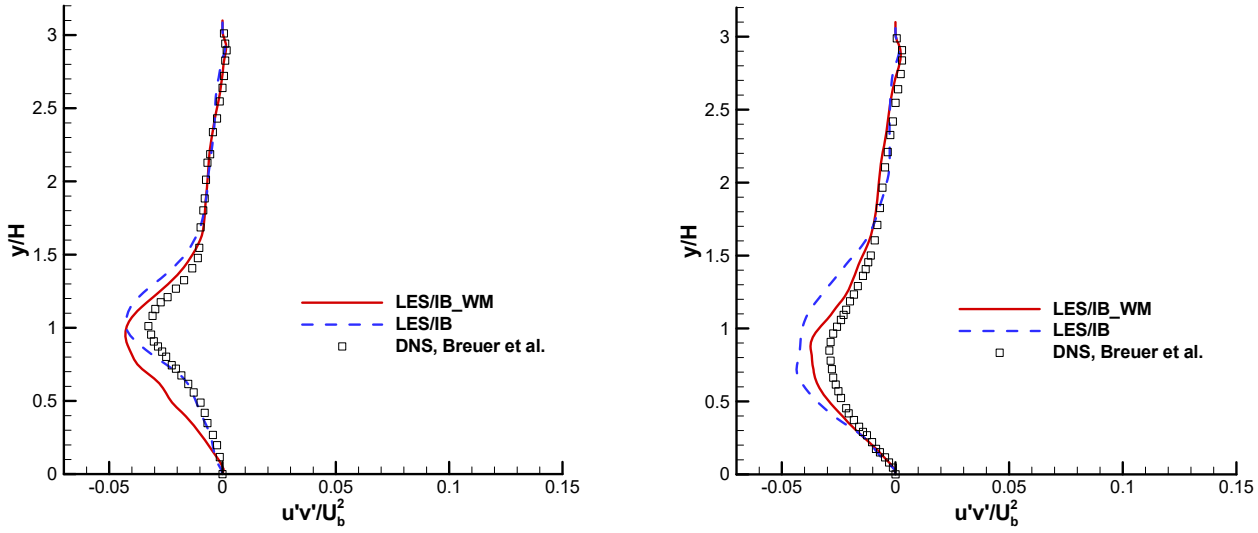

(a) (b)

Figure 10 Mean streamwise velocity $\langle u \rangle$ at Re = 10,595, (a) $x / h = 0.5$ (b) $x / h = 2$ (c) $x / h = 4$ (d) $x / h = 6$ (see online version for colours)

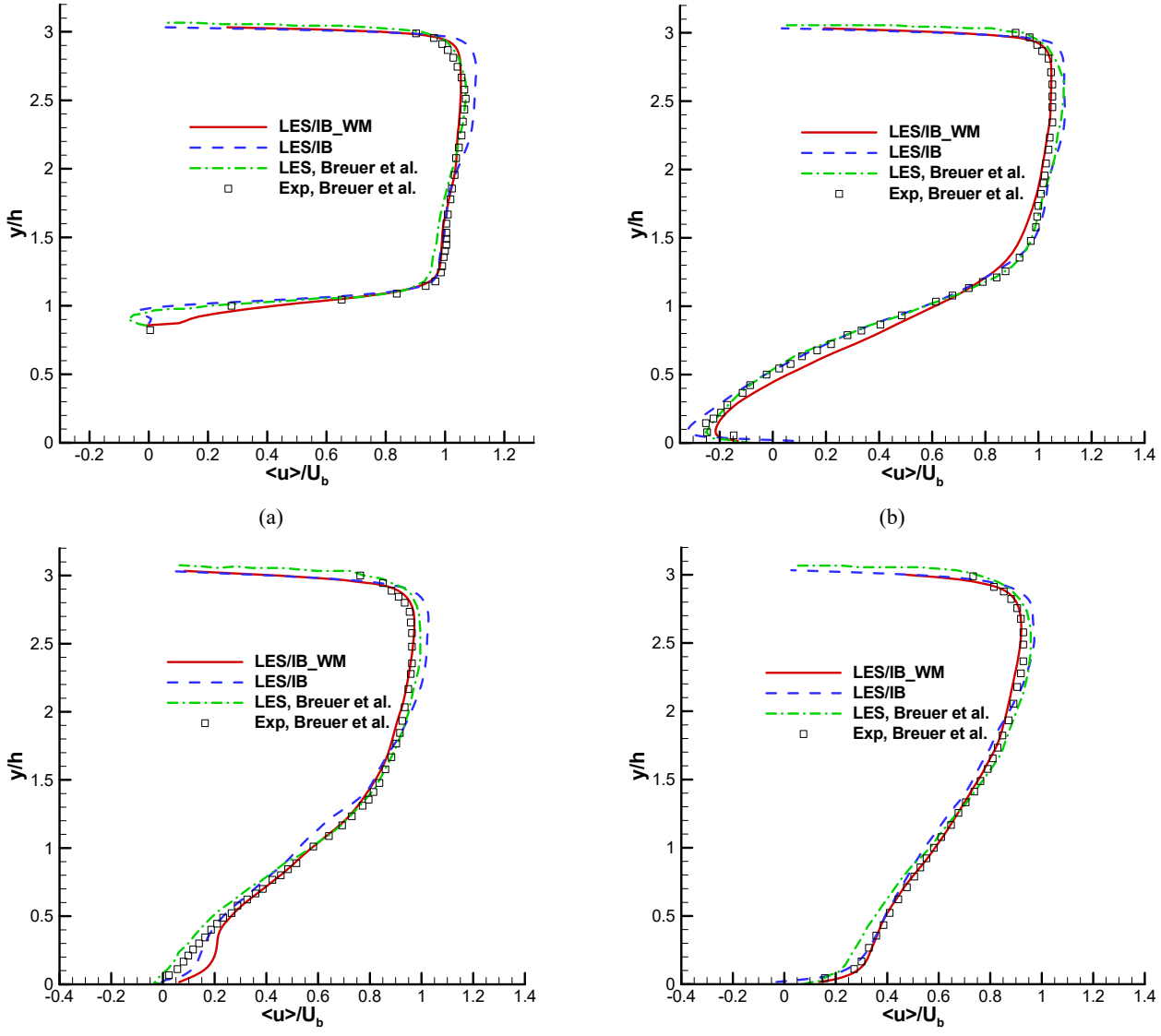

(a) (b)

(c) (d)

Figure 11 Mean transverse velocity <*v*> at Re = 10,595, (a) *x* / *h* = 0.5 (b) *x* / *h* = 2 (c) *x* / *h* = 4 (d) *x* / *h* = 6 (see online version for colours)

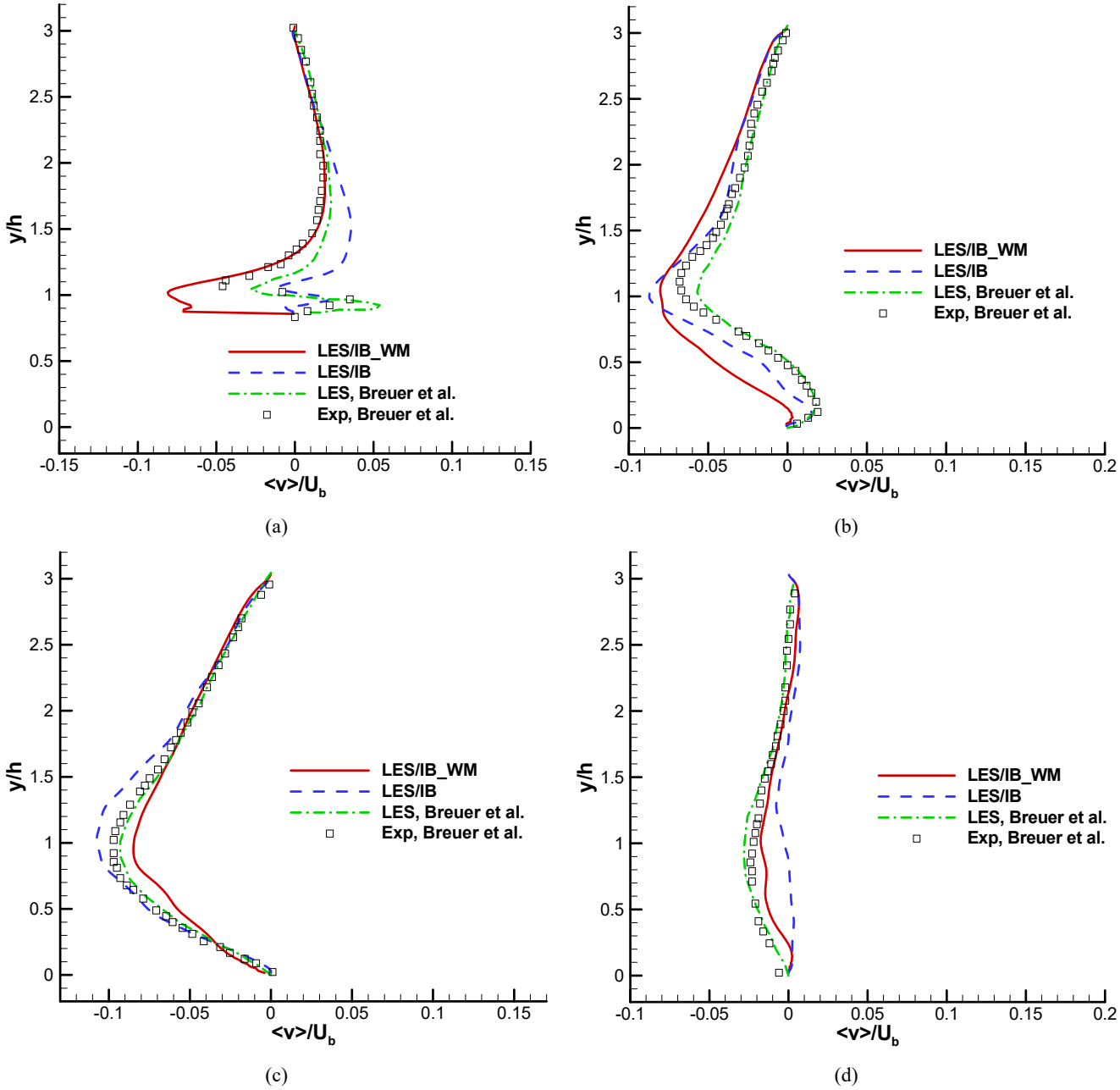

5 Summary and conclusions

In this paper, an IB method is extended to LES of turbulent flows. To alleviate the requirement of mesh resolution in the vicinity of the wall, wall modelling technique is utilised in the treatment of the IB.

Instead of the no-slip boundary condition, the no-penetration condition and the wall shear stress yielded by the wall modelling technique are enforced at the IB to evaluate the velocity at an IB node. With the employment of a local modified coordinate system, the simplified TBLE is solved only in one tangential direction.

To validate the present LES/IB method, several numerical experiments have been carried out. The predicted profiles of mean velocity or turbulence intensity are compatible with the published experimental data and/or numerical results. Especially, for the massively separated flow over periodic hills, the results obtained with wall modelling are somewhat closer to the referenced results than those without wall modelling. This indicates the necessity of incorporation of the wall modelling technique.

Acknowledgements

This work has been supported by the National Natural Science Foundation of China under Grant 11972191.

References

Baggett, J.S., Jiménez, J. and Kravchenko, A. (1997) 'Resolution requirements in large-eddy simulation of shear flows', *CTR Annual Research Briefs*, pp.51–66.

Balaras, E., Benocci, C. and Piomelli, U. (1996) 'Two layer approximate boundary conditions for large-eddy simulations', *AIAA Journal*, Vol. 34, No. 6, pp.1111–1119.

Belov, A., Martnelli, L. and Jameson, A. (1997) *Three-dimensional Unsteady Incompressible Flow Computations Using Multigrid*, AIAA Paper 1997-0443..

Borazjani, I. (2013) 'Fluid-structure interaction, immersed boundary-finite element method simulations of bio-prosthetic heart valves', *Computer Methods in Applied Mechanics and Engineering*, 15 April, Vol. 257, pp.103–116.

Borazjani, I. and Sotiropoulos, F. (2008) 'Numerical investigation of the hydrodynamics of carangiform swimming in the transitional and inertial flow regimes', *Journal of Experimental Biology*, Vol. 211, No. 10, pp.1541–1558.

Bose, S.T., Moin, P. and You, D. (2010) 'Grid-independent large-eddy simulation using explicit filtering', *Physics of Fluids*, Vol. 22, No. 10, p.105103.

Breuer, M., Peller, N., Rapp, C.H. and Manhart, M. (2009) 'Flow over periodic hills-numerical and experimental study in a wide range of Reynolds number', *Computers and Fluids*, Vol. 38, No. 2, pp.433–457.

Cabot, W. and Moin, P. (2000) 'Approximate wall boundary conditions in the large-eddy simulation of high Reynolds number flow', *Flow, Turbulence and Combustion*, Vol. 63, No. 1, pp.269–291.

Capizzano, F. (2011) 'Turbulent wall model for immersed boundary methods', *AIAA Journal*, Vol. 49, No. 11, pp.2367–2381.

Chen, Z.L., Hickel, S. and Devesa, A. (2014) 'Wall modeling for implicit large-eddy simulation and immersed-interface methods', *Theoretical and Computational Fluid Dynamics*, Vol. 28, No. 1, pp.1–21.

Dadone, A. and Grossman, B. (2007) 'Ghost-cell method for analysis of inviscid three-dimensional flows on Cartesian-grids', *Computer &Fluids*, Vol. 36, No. 10, pp.1513–1528.

Deleon, R., Sandusky, M. and Senocak, I. (2018) 'Simulations of turbulent flow over complex terrain using an immersed-boundary method', *Boundary-Layer Meteorol*., 15 April, Vol. 167, pp.399–420.

Germano, M., Piomelli, U., Moin, P. et al. (1991) 'A dynamic subgrid-scale eddy viscosity model', *Physics of Fluids*, Vol. 3, No. 7, pp.1760–1765.

Gilmanov, A., Sotiropoulos, F. and Balaras, E. (2003) 'A general reconstruction algorithm for simulating flows with complex 3D immersed boundaries on Cartesian grids', *Journal of Computational Physics*, Vol. 191, No. 2, pp.660–669.

Iaccarino, G. and Verzicco, R. (2003) 'Immersed boundary technique for turbulent flow simulations', *Applied Mechanics Reviews*, Vol. 56, No. 3, pp.331–347.

Lourenco, L.M. and Shih, C. (1993) 'Characteristics of the plane turbulent near wake of a circular cylinder, a particle image velocimetry study', *Private Communication*, (data taken from Reference 'Kravchenko, A.G. and Moin, P. (2000) 'Numerical studies of flow over a circular at Re_D = 3,900', *Physics of Fluids*, Vol. 12, No. 2, pp.403–417).

Ma, X., Karamanos, G.S. and Karniadakis, G.E. (2000) 'Dynamics and low-dimensionality of a turbulent near wake', *Journal of Fluid Mechanics*, 10 May, Vol. 410, pp.29–65.

Mavriplis, D.J. and Jameson, A. (1990) 'Multigrid solution of the Navier-Stokes equations on triangular meshes', *AIAA Journal*, Vol. 28, No. 8, pp.1415–1425.

Meneveau, C., Lund, T.S. and Cabot, W.H. (1996) 'A Lagrangian dynamic subgrid-scale model of turbulence', *Journal of Fluid Mechanics*, 25 July, Vol. 319, pp.353–385.

Meyer, M., Hickel, S. and Adams, N.A. (2010) 'Assessment of implicit large-eddy simulation with a conservative immersed interface method for turbulent cylinder flow', *International Journal of Heat and Fluid Flow*, Vol. 31, No. 3, pp.368–377.

Mittal, R. and Iaccarino, G. (2005) 'Immersed boundary methods', *Annual Review of Fluid Mechanics*, Vol. 37, No. 1, pp.239–261.

Ng, E.Y.K., Tan, H.Y., Lim, H.N. and Choi, D. (2004) 'Incorporation of Cabot's wall functions in RANS with applications in turbomachinery', *Progress in Computational Fluid Dynamics, An International Journal*, Vol. 4, No. 6, pp.309–319.

Nithiarasu, P. (2003) 'An efficient artificial compressibility (AC) scheme based on the characteristic based split (CBS) method for incompressible flows', *International Journal for Numerical Methods in Fluids*, Vol. 56, No. 13, pp.1815–1845.

Parnaudeau, P., Carlier, J., Heitz, D. et al. (2008) 'Experimental and numerical studies of the flow over a circular cylinder at Reynolds number 3900', *Physics of Fluids*, Vol. 20, No. 8, p.085101.

Peskin, C.S. (1972) 'Flow patterns around heart valves: a numerical method', *Journal of Computational Physics*, Vol. 10, No. 2, pp.252–271.

Pu, T.M. and Zhou, C.H. (2018) 'An immersed boundary/wall modeling method for RANS simulation of compressible turbulent flows', *International Journal for Numerical Methods in Fluids*, Vol. 87, No. 5, pp.217–238.

Pu, T.M., Zhou, C.H. and Ai, J.Q. (2019) 'Extension of the local domain-free discretization method to large eddy simulation of turbulent flows', *International Journal for Numerical Methods in Fluids*, Vol. 90, No. 9, pp.456–478.

Sarkar, S. and Sarkar, S. (2010) 'Simulation of vortex dynamics in a cylinder wake by the immersed boundary technique', *Progress in Computational Fluid Dynamics, An International Journal*, Vol. 10, No. 3, pp.129–145.

Schumann, U. (1975) 'Subgrid scale model for finite difference simulations of turbulent flows in plane channels and annuli', *Journal of Computational Physics*, Vol. 18, No. 4, pp.376–404.

Senturk, U., Brunner, D., Jasak, H. et al. (2019) 'Benchmark simulations of flow past rigid bodies using an open-source, sharp interface immersed boundary method', *Progress in Computational Fluid Dynamics, An International Journal*, Vol. 19, No. 1, pp.205–219.

Shi, B.J., Yang, X.L., Jin, G.D. et al. (2019) 'Wall-modeling for large-eddy simulation of flows around an axisymmetric body using the diffuse-interface immersed boundary method', *Journal of Applied Mathematics and Mechanics-English Edition*, Vol. 40, No. 3, pp.305–320.

Tessicini, F., Iaccarino, G., Fatica, M. et al. (2002) 'Wall modeling for large-eddy simulation using an immersed boundary method', *CTR Annual Research Briefs*, pp.181–187.

Werner, H. and Wengle, H. (1991) 'Large-eddy simulation of turbulent flow over and around a cube in a plate channel', *8th Symposium on turbulent Shear Flows*, pp.155–168.

Zhang, Y. and Zhou, C.H. (2014) 'An immersed boundary method for simulation of inviscid compressible flows', *International Journal for Numerical Methods in Fluids*, Vol. 74, No. 11, pp.775–793.

Zhou, C.H. and Shu, C. (2009) 'A local domain-free discretization method to simulate three-dimensional compressible inviscid flows', *International Journal for Numerical Methods in Fluids*, Vol. 61, No. 9, pp.970–986.

Zhou, C.H. and Shu, C. (2011) 'A local domain-free discretization method for simulation of incompressible flows over moving bodies', *International Journal for Numerical Methods in Fluids*, Vol. 66, No. 2, pp.162–182.

Nomenclature

C_s	SGS model coefficient
$\overline{c}_d$	Mean drag coefficient
$\overline{c}_{pb}$	Mean back pressure coefficient
$\mathbf{F}$	Convective flux tensor
$\mathbf{G}$	Viscid flux tensor
$\mathbf{I}^m$	Modified identity matrix
L	Referenced length
L_r	Mean recirculation length
$\overline{p}$	Filtered pressure
Re	Reynolds number
S_t	Strouhal number
U	Referenced velocity
$\overline{u}_i$	Filtered Cartesian velocity
ν	Molecular kinetic viscosity
ν_t	Eddy viscosity
$\mathbf{w}$	Vector of flow variables
Δt	Physical time step
τ_w	Wall shear stress
$\langle u \rangle$, $\langle v \rangle$	Mean velocities
$\langle u' u' \rangle$, $\langle v' v' \rangle$	Mean normal Reynolds stresses
$\langle u'v' \rangle$	Mean Reynolds shear stress